Flux-resolved Spectropolarimetric Evolution of the X-Ray Pulsar Hercules X-1 Using IXPE

Garg, Akash; Rawat, Divya; Bhargava, Yash; Méndez, Mariano; Bhattacharyya, Sudip

Published in:
Astrophysical Journal Letters

DOI:
10.3847/2041-8213/acccfa

Publication date:
2023

The Astrophysical Journal Letters, 948:L10 (7pp), 2023 May 1 https://doi.org/10.3847/2041-8213/acccfa

Flux-resolved Spectropolarimetric Evolution of the X-Ray Pulsar Hercules X-1 Using IXPE

Akash Garg[1], Divya Rawat[1], Yash Bhargava[2], Mariano Méndez[3], and Sudip Bhattacharyya[2]
[1] Inter-University Center for Astronomy and Astrophysics, Ganeshkhind, Pune 411007, India; akash.garg@iucaa.in
[2] Department of Astronomy and Astrophysics, Tata Institute of Fundamental Research, 1, Homi Bhabha Road, Colaba, Mumbai 400005, India
[3] Kapteyn Astronomical Institute, University of Groningen, PO BOX 800, Groningen NL-9700 AV, The Netherlands
Received 2023 April 3; revised 2023 April 10; accepted 2023 April 12; published 2023 May 5

Abstract

We conduct a spectropolarimetric study of the accreting X-ray pulsar Hercules X-1 using observations with the Imaging X-ray Polarimetry Explorer (IXPE). IXPE monitored the source in three different epochs, sampling two "Main-on" and one "Short-on" state of the well-known super-orbital period of the source. We find that the 2–7 keV polarization fraction increases significantly from ∼7% to 9% in the Main-on state to ∼15%–19% in the Short-on state, while the polarization angle remains more or less constant or changes slightly, ∼47°–59°, in all three epochs. The polarization degree and polarization angle are consistent with being energy independent for all three epochs. We propose that in the Short-on state, when the neutron star is partially blocked by the disk warp, the increase in the polarization fraction can be explained as a result of the preferential obstruction of one of the magnetic poles of the neutron star.

Unified Astronomy Thesaurus concepts: Spectropolarimetry (1973); X-ray astronomy (1810); High energy astrophysics (739); Accretion (14); Stellar accretion disks (1579)

1. Introduction

Hercules X-1 (Her X-1) is an accreting X-ray binary pulsar with a low-mass companion, HZ Her, discovered in the 1970s (Shklovskij & Efremov 1972; Tananbaum et al. 1972). The lightcurve of Her X-1 shows pulsations at the neutron star (NS) spin period of 1.24 s (Staubert et al. 2013) and clear dips due to occultation by the companion at 1.7 day intervals (Staubert et al. 2013; Leahy & Abdallah 2014), indicating that the source has a high inclination (>80°; Deeter et al. 1981). Additionally, the source is known to show a super-orbital period of 34.85 days (Giacconi et al. 1973), which is assumed to occur due to a warp in the accretion disk around the NS (Petterson et al. 1991; Leahy 2002). The super-orbital period is characterized by two high-flux states, "Main-on" and "Short-on," with two "Off" states in between (Staubert et al. 2013; Leahy & Wang 2020).

The broadband spectrum of Her X-1 is known to arise from multiple regions around the NS (Becker & Wolff 2007; Abdallah & Leahy 2015; Kosec et al. 2022). The hard X-ray pulsating emission (> 2 keV) originates from the accretion column, while the soft X-ray emission (< 1 keV) comes from the reprocessed flux of the accretion column radiation. The column density of the interstellar matter toward Her X-1 is low (5×10^{19} cm^{-2}; dal Fiume et al. 1998), and the spectrum of the source exhibits an evolving cyclotron resonant scattering feature (35–42 keV; Gruber et al. 2001; Fürst et al. 2013; Ji et al. 2019; Bala et al. 2020), indicative of the high NS magnetic field. Her X-1 exhibits a highly asymmetric pulse profile that is dependent on the super-orbital period (Leahy 2004). The evolution of the pulse phase in the Main-on and the Short-on states suggests that the emission from the closest magnetic pole is a pencil beam, whereas that of the farthest pole is a fan beam (Scott et al. 2000; Leahy 2004).

Although the X-ray spectral and temporal properties of Her X-1 have been extensively studied to investigate the configuration and emission regions, there remains a degeneracy of the models. Through polarimetric observations, it is possible to delve into the geometry of the accretion column and magnetic field and examine the changes in polarization during the super-orbital phase. Recent work by Doroshenko et al. (2022) has explored the soft X-ray polarization properties of Her X-1 using the Imaging X-ray Polarimetry Explorer (IXPE) during the Main-on state (phase range 0.0–0.2 of the super-orbital period), revealing an energy-independent polarization in the 2–7 keV range that strongly depends on the pulse phase. They report a significant X-ray polarization degree (PD) of $8.6\% \pm 0.5\%$ at a polarization angle (PA) of $62^\circ \pm 2^\circ$, which was much lower than the theoretically expected value (Caiazzo & Heyl 2021). They further speculated three possible reasons for this low PD value: (1) radiative transfer in the magnetized plasma within the emission region; (2) propagation of the initially polarized X-rays through the NS magnetosphere; and (3) the effect of the combination of the emission from the two magnetic poles.

In this Letter, we present a comparison of the polarization properties of Her X-1 in the Main-on and Short-on states of the super-orbital phase as seen by IXPE at three different epochs. The goal of this study is to explore how the accretion disk warping affects polarization. The methods and data analysis procedures for the observations are outlined in Section 2, and the results and ensuing discussion are reported in Sections 3 and 4, respectively.

2. Observation and Data Analysis

IXPE (Weisskopf et al. 2022) is NASA's dedicated X-ray polarimetry mission, launched on 2021 December 9 from the Kennedy Space Center. It has on board three identical units of Gas Pixel detectors, DU1, DU2, and DU3 (Baldini et al. 2021). These units independently record the spatial, time, and energy-

Table 1
Log of the Observations with the Time-averaged PA and PD for Her X-1 with PCUBE and XSPEC Model CONSTANT*POLCONST*NTHCOMP for All the Three Epochs

Epoch	ObsID	Parameter	PCUBE All DUs	XSPEC
1	01001899	PA (deg)	59.2 ± 1.5	59.3 ± 1.7
		PD (%)	7.5 ± 0.4	8.5 ± 0.5
2	02003801	PA (deg)	46.6 ± 3.4	44.2 ± 2.7
		PD (%)	17.3 ± 2.0	19.0 ± 1.8
3	02004001	PA (deg)	49.8 ± 1.9	50 ± 1.8
		PD (%)	8.2 ± 0.5	7.8 ± 0.5

resolved polarimetric information in the 2–8 keV band (Di Marco et al. 2022). IXPE observed the X-ray pulsar Her X-1 at three different epochs, 2022 February 17–24, 2023 January 18–21, and 2023 February 3–8. The observation IDs for all epochs are given in Table 1. If not stated otherwise, all reported errors indicate the 1σ confidence (68%) range for the associated parameter.

The upper and lower panels of Figure 1 show the Swift/BAT and MAXI lightcurves of Her X-1 in the 15–50 keV and 4–10 keV energy bands, respectively. Both lightcurves exhibit the well-known ∼35 day super-orbital period of the source. In the first and third IXPE Epochs, the source was in the Main-on state (gray and green shaded regions in Figure 1, respectively), which marks the start of the super-orbital cycle. In the second IXPE epoch, Her X-1 was detected in the Short-on state (pink shaded region in Figure 1). Throughout each epoch, there are brief intervals of eclipsing by the donor star and pre-eclipsing dips caused by obscuration due to the accretion stream from the donor star (Igna & Leahy 2012; Doroshenko et al. 2022). We discard all such dips to conduct the analysis and generate multiple segments for each epoch, facilitating a time-dependent investigation of the polarization properties. Further, we extract a merged cleaned event file (to combine the different segments to create a single event file per epoch) using the HEASOFT tool XSELECT to determine the time-averaged polarization properties.

The polarimetric analysis is carried out using the software suite IXPEOBSSIM 29.2.0[4] (Baldini et al. 2022), which is equipped with various tools to process IXPE level2 event files and produce scientific results. For each individual segment and for the merged event file in each epoch, we procure the source and background cleaned event files for all DUs using the XPSELECT tool. We choose a circular region (radius of 60″) and an annular region (inner and outer radii of 180″ and 240″) for the extraction of source and background events, respectively. Based on the formalism developed by Kislat et al. (2015), the tool XPBIN assists in binning the event files to generate the polarization cubes, count I and Stokes Q and U , spectra using algorithms like PCUBE, PHA1, PHAQ, and PHAU, respectively (for more details, also see Muleri 2022; Rawat et al. 2023). Owing to uncertainties in the 7–8 keV band (Doroshenko et al. 2022), all the binned products are estimated in the 2–7 keV energy range using the response matrices version v012 of IXPEOBSSIM.

Using the HEASOFT tool FTGROUPPHA, we have rebinned the I, Q, and U spectra. Specifically, we first rebin the I spectrum uniformly by a factor of 2 for Epochs 1 and 3 and by a factor of 3 for Epoch 2, and then rebin the Q and U spectra using the binning of the I spectrum as a template. The spectropolarimetric fitting is conducted using the X-ray spectral fitting package XSPEC VERSION 12.13.0 (Arnaud 1996). Doroshenko et al. (2022) remarked in their work that during Epoch 1, there is an additional vignetting due to the offset in the pointing direction of IXPE telescopes and due to uncertainties in boom motion modeling that can influence effective area calibration and thereby the spectral analysis. They also noted that this would not affect the polarization measurements as the Stokes spectra U and Q are normalized by the I flux, which in turn make up for the systematic uncertainties coming from the effective area. No information on offset or other uncertainties is available for Epoch 2 and 3 data.

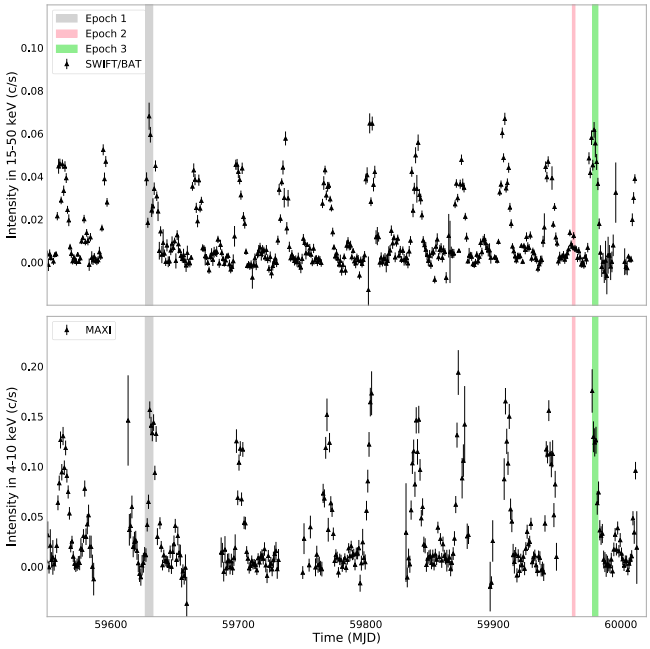

Figure 1. Swift/BAT (upper panel) and MAXI (lower panel) lightcurve of Her X-1 in the 15–50 keV and 4–10 keV bands, respectively. The shaded area represents the duration of the IXPE observations of the source.

3. Results

3.1. Polarization Measurements with IXPE

Using a model-independent analysis (PCUBE algorithm), we estimate significant polarization in the source at all three epochs. We find that for Epoch 1, the PD is $7.5\% \pm 0.4\%$ at a PA of $59^\circ \pm 1^\circ.5$ in the 2–7 keV band for all three DUs. At Epoch 2, we find that the PD has increased to $17.3\% \pm 2.0\%$ with the PA decreasing to $46^\circ.6 \pm 3^\circ.4$ (in 2–7 keV for all 3 DUs) and at Epoch 3 the PD is at $8.2\% \pm 0.5\%$ at a PA of $49^\circ.8 \pm 1^\circ.9$. The PD and PA, as seen in the first Epoch, are consistent with Doroshenko et al. (2022) within 2σ confidence level with the minor differences arising possibly due to the update in the calibration or differences in the choice of the time segments for averaging. The PD increases from Epoch 1 to 2 and then decreases from Epoch 2 to 3, with the values in Epochs 1 and 3 being consistent with each other. We depict the contour plot of the time-averaged polarization parameters, PD, PA, and the Stokes parameters, Q/I and U/I, in the 2–7 keV energy range for all three epochs in Figure 2. We note that the uncertainties of the PD and PA are calculated assuming that the

[4] https://ixpeobssim.readthedocs.io/en/latest/overview.html

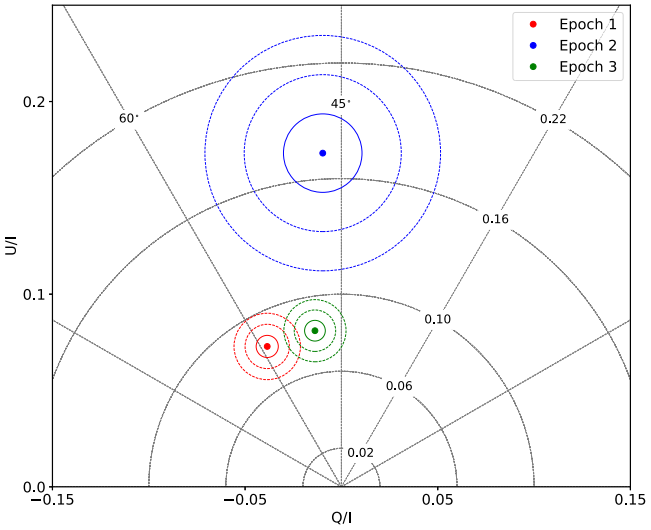

Figure 2. The PD (azimuthal lines), PA (radial lines), and normalized Stokes parameters, Q/I (x-axis) and U/I (y-axis), of Her X-1 for the three epochs (please see legends) with IXPE. The measurements were obtained using the PCUBE tool in the 2–7 keV band. The contours are at 68.27%, 95.45%, and 99.73% confidence levels for both Stokes parameters.

Stokes parameters Q/I and U/I are normally distributed and uncorrelated and that the PD and PA are independent (Kislat et al. 2015). Table 1 lists the values of time-averaged PA and PD, combining all detector units at each epoch.

Next, we estimate the time-averaged PA and PD in four energy bands, 2–2.74 keV, 2.74–3.74 keV, 3.74–5.12 keV, and 5.12–7 keV, for all DUs to study their energy dependence as shown in Figure A1. From this figure, it is apparent that the polarization parameters are independent or weakly dependent on energy in all three epochs (similar to Doroshenko et al. 2022, for Epoch 1). We also calculate the PA and PD parameters for each segment of all epochs to examine the time dependence of the observed polarization. Figure 3 shows the time evolution of the PA and PD for all three epochs, with the source lightcurve shown in gray. For all epochs, both PA and PD are consistent with a constant throughout each epoch. This figure also shows an increase in the PD in the low-flux state compared to the two high-flux states, although it is difficult to discern this from these plots due to the large error bars. But the time-averaged results, as seen in Table 1, show that the differences are significant. The segment-wise values of the PA and PD for all DUs are given in Table A1.

3.2. Spectropolarimetric Analysis

Besides the PCUBE approach to study the polarization properties, we undertake a separate approach as well where we fit the I, Q, and U spectra of all IXPE detectors in the 2–7 keV energy band simultaneously in XSPEC. Essentially, the idea is to model the I spectrum to determine the radiative mechanism in conjunction with a polarization XSPEC model for the Q and U spectra to trace the energy dependence of the polarization parameters (PD and PA). The source spectrum in the 2–7 keV energy band can be well described by a single power law with a cutoff at ∼20 keV to account for the accretion column emission (Kosec et al. 2022). However, Doroshenko et al. (2022) have modeled the radiative mechanism with NTHCOMP and found that the polarization is consistent with a constant (on modeling it with POLCONST).

In this work, we first fit the time-averaged I, Q, and U spectra for all three epochs using the model CONSTANT*POLCONST*POWERLAW. Since we find that the source polarization is energy independent (Figure A1), we model the Stokes spectra using the multiplicative model POLCONST. The multiplicative factor CONSTANT takes into account possible energy-independent uncertainties in the cross-calibration of the three IXPE detectors. The spectral fitting gives a χ^2/dof of 713/552, 408/363, and 1154/552 for Epochs 1, 2, and 3, respectively. We keep all the parameters free (i.e., A: the polarization fraction, *psi*: the polarization angle, Γ: power-law index, and norm: power-law Norm) during the fitting. The high reduced χ^2 of the I spectra suggests that a simple power-law model cannot describe the spectra adequately, and a different model is needed to explain the emission from the accretion column.

Following Doroshenko et al. (2022), we replace the POWERLAW component with the component NTHCOMP in XSPEC, assuming a disk-blackbody seed-photon source; this component computes the Comptonization of seed photons of temperature $kT_{\rm bb}$ by nonrelativistic electrons in a corona of temperature kT_e. This model yields better spectral fitting with χ^2/dof for the three epochs of 606/550, 382/361, and 699/550. All the parameters are kept free to vary during the fitting but are linked across the I, Q, and U spectra. For Epoch 1, we estimate the best-fit values of $\mathrm{PD} = 8.5\% \pm 0.5\%$, $\mathrm{PA} = 59\overset{\circ}{.}3 \pm 1\overset{\circ}{.}7$, $\Gamma = 1.29 \pm 0.04$, $kT_e = 5.75 \pm 1.55$ keV, $kT_{\rm bb} = 0.58 \pm 0.03$ keV, and $\mathrm{norm} = 0.111 \pm 0.002$. All the values except that of $kT_{\rm bb}$ are consistent with the values found by Doroshenko et al. (2022, see their Supplementary Table 1). The best-fit PA and PD values for all epochs are given in Table 1. These values agree with what we get from the PCUBE method within 1σ errors, thereby confirming that there is indeed a change in the polarization parameters when the source was in the low-flux state. The best-fit spectral slope of the spectrum, Γ, changes from 1.29 ± 0.04 in Epoch 1 to 1.14 ± 0.07 in Epoch 2 and to 1.22 ± 0.01 in Epoch 3. The changes are marginally significant, and the values are consistent within 3σ. Owing to the limited energy range of the data, 2–7 keV, kT_e, and $kT_{\rm in}$ have large error bars and thereby it is difficult to assess whether there is any change. Particularly, kT_e and $kT_{\rm in}$ are respectively measured to be 10.2 ± 14.5 keV and <0.63 keV for Epoch 2 and 7.43 ± 0.25 and <0.31 for Epoch 3. It is important to point out here that the underlying mechanism responsible for the emission of the accretion column in Her X-1 is likely Comptonization by the bulk motion of electrons, which is not the mechanism used by NTHCOMP. But as Doroshenko et al. (2022) mentioned, the I spectrum in the modest IXPE energy range of 2–7 keV can be modeled with a simple NTHCOMP component only to track the change of the spectral shape between epochs. In any case, the PA and PD estimates are not affected by the choice of the radiative model.

Figure 4 shows the jointly fitted I (top left panel), Q (middle left panel), and U (bottom left panel) spectra for all three DUs along with their residuals in the adjacent right panels for Epoch 2. We also fit the I, Q, and U spectra of each segment in all epochs with the model combination CONSTANT*POLCONST*POWERLAW to test whether there was any evolution of PA/PD or the spectral parameters. The reduced χ^2 ranges from 0.98 to 1.14 for Epoch 1, 0.89 to 1.17 for Epoch 2, and 0.84 to 1.17 for Epoch 3. Within 3σ limit, the values of PA and PD are consistent with being constant to ∼8% and ∼60° for Epoch 1,

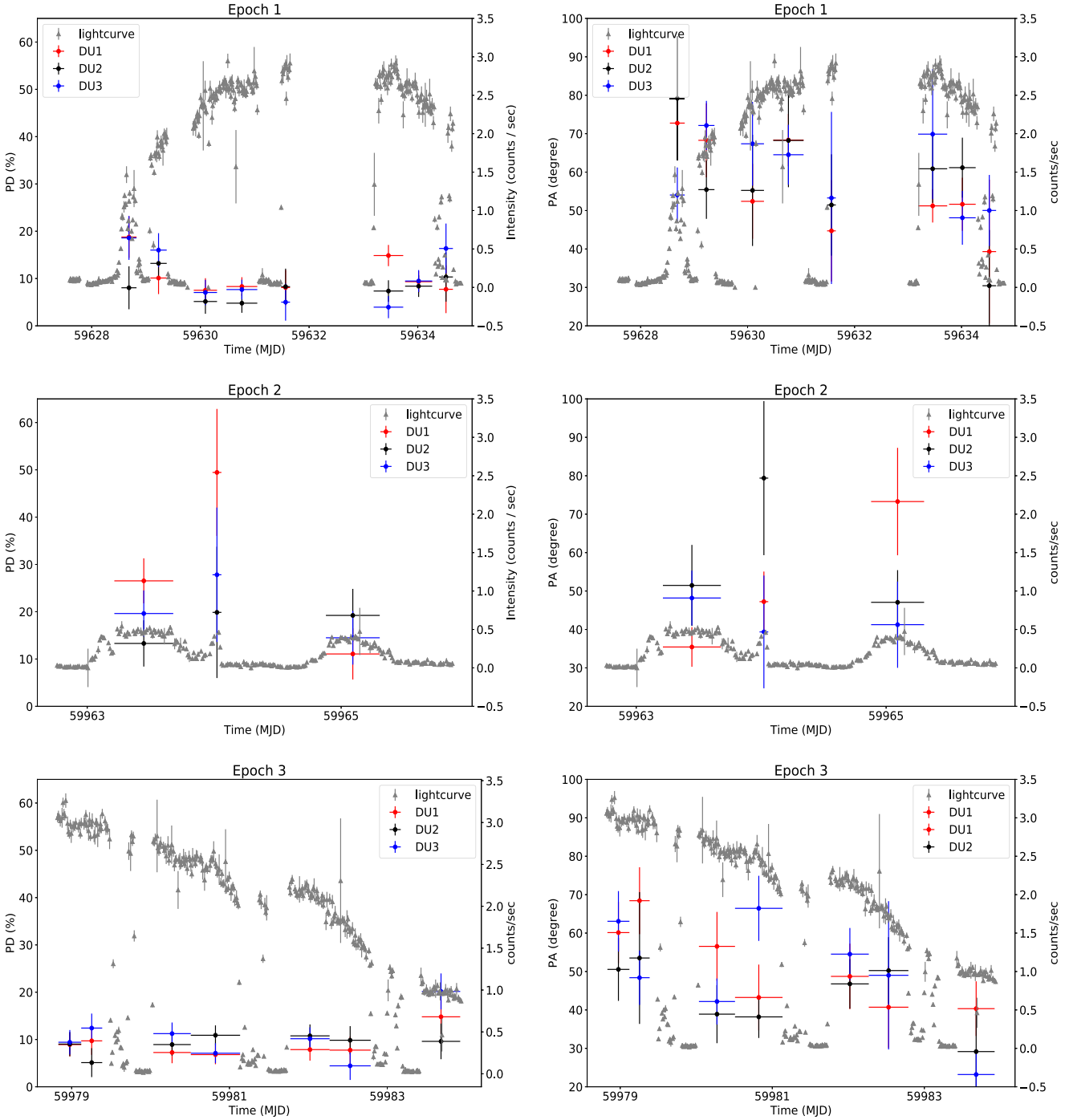

Figure 3. PD (left), PA (right), and IXPE photon counts (gray points) of Her X-1 as a function of time for the three epochs. The red, black, and blue symbols represent the data from DU1, DU2, and DU3, respectively.

∼18% and ∼45° for Epoch 2, and ∼10% and ∼50° for Epoch 3. This resembles what we found with the PCUBE method in Figure 3. The spectral slope seems to vary at 3σ in positive correlation with the count rate for Epoch 1 but for Epochs 2 and 3, it is constant around ∼0.8 and ∼1.0. Table A1 gives the values of all spectral parameters for all segments.

4. Discussion and Conclusions

We present, for the first time, a significant increase in the PD of the accreting X-ray pulsar Her X-1, from 7% to 9% in the high-flux state (Main-on) to 15%–19% in the low-flux state (Short-on) within its super-orbital period. For the first Epoch, when the source was in the Main-on phase, the polarimetric and spectropolarimetric analysis yields a polarization angle of 57°–61°. These values are consistent with the values reported by Doroshenko et al. (2022) for the same observation. For the second Epoch, i.e., the Short-on state, the polarization angle is 39°–50°. In the third Epoch, when the source is again in the Main-on state, the polarization angle is 47°–52°. Within 3σ, the polarization angle for all three epochs is the same. We further find that there is no significant energy dependence of the polarization fraction and polarization angle in any of our epochs (upper panel of Figure A1). These results are consistent

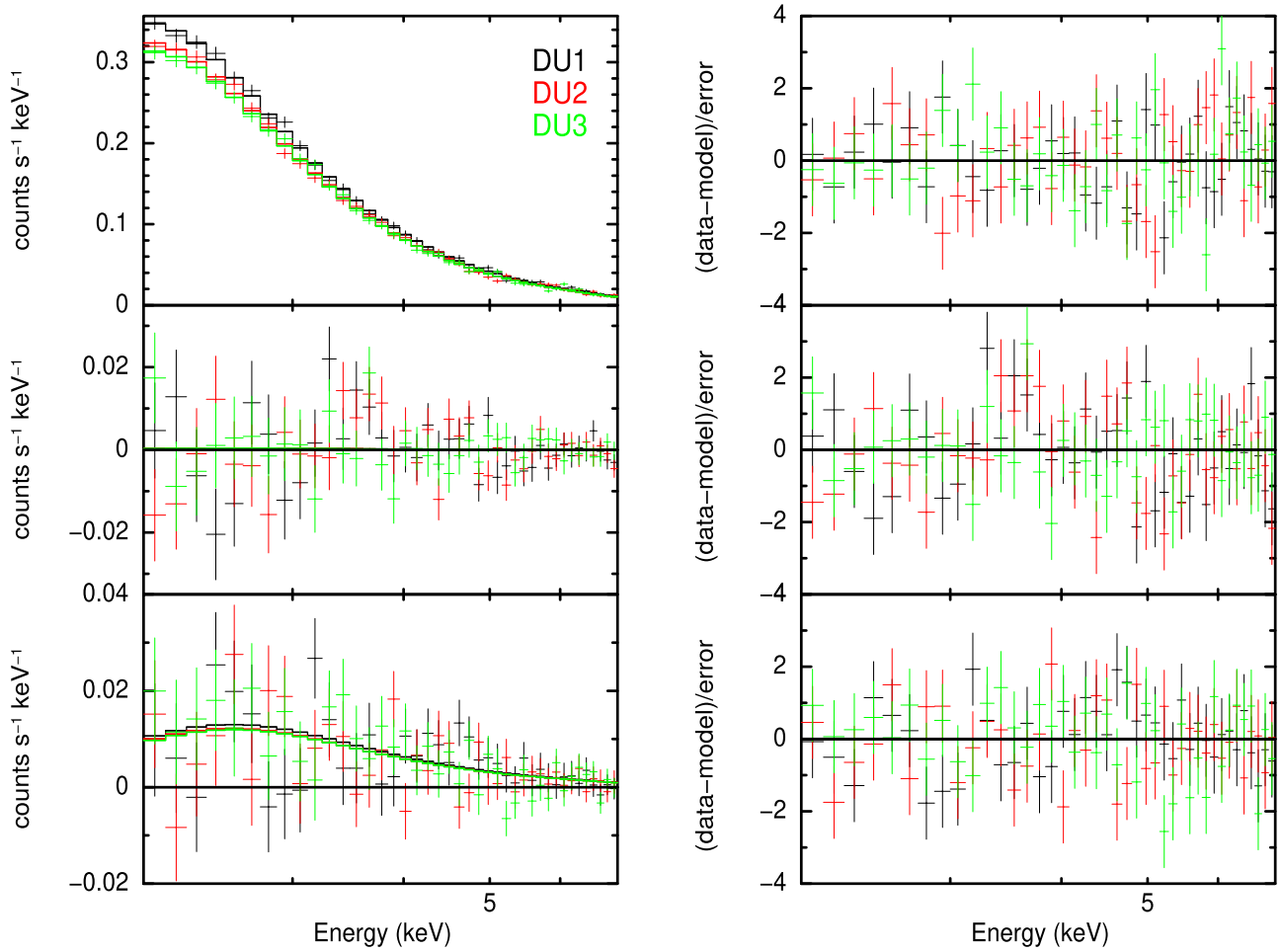

Figure 4. The simultaneous IXPE *I* (top left panel), *Q* (middle left panel), and *U* spectra (bottom left panel) of Her X-1 fitted with the model CONSTANT∗POLCONST∗NTHCOMP for Epoch 2. The right panels show the respective residuals of the best-fitting model to the data. The black, red, and green symbols represent the data from DU1, DU2, and DU3, respectively.

with Doroshenko et al. (2022) but in contrast with predictions of Caiazzo & Heyl (2021).

During the Main-on state, the X-ray emission comes from the NS and the tilted accretion disk, whereas in the Short-on state, the disk blocks the NS partially and most of the emission originates from the inner regions of the disk (Petterson et al. 1991; Scott et al. 2000; Leahy 2002). Using data from two super-orbital phases, our results show, for the first time, that the PD increases during the low-flux phase of the super-orbital period, i.e., when the central source is more obstructed by the disk warp. The possible reasons for this increase in the PD could be (1) the obscuring structure adds to the PD, (2) the obscuring structure blocks more the unpolarized than the polarized emission, and (3) the obscuring structure obstructs preferentially the emission from one of the magnetic poles of the NS, thus making the emission more single pole-like and hence increasing the net PD. The first option does not appear to be plausible because if the polarization originates from the accretion column, an obscuring warp, far from the NS, should not increase but decrease the PD. The second option is also unlikely because if we assume that the polarized emission is due to a nonthermal power-law component (which is the only dominant component) in the 2–7 keV band, then the additional obstruction of an unpolarized component (if any) may therefore not change the PD. Thus, option 3 appears to be the most plausible of the three. If this is the case this result can potentially put a constraint on the geometry of both the warp and the accretion column.

Considering the spectral model of Becker & Wolff (2005), Caiazzo & Heyl (2021) computed the expected polarized emission of Her X-1, and predicted both phase- and energy-dependent polarization of 60%–80% in the 1–10 keV band. On the contrary, using both the model-independent and the spectropolarimetric methods, here we found that the maximum polarization fraction of Her X-1 is in the range 15%–19%; this high PD was observed during the Short-on state. Our phase-resolved analysis results (see the left panel of Figure 3 and Table A1) further exclude the possibility that, during these IXPE observations, the PD of Her X-1 was larger than this. In this context, it is worth developing models of the emission of the accretion column in X-ray binary pulsars. This, plus further observations of the X-ray polarimetric properties of Her X-1 in other phases of its super-orbital period could shed more light on the accretion geometry in X-ray pulsars.

The authors thank the anonymous reviewer for constructive comments to improve the manuscript. This research used data products provided by the IXPE Team (MSFC, SSDC, INAF, and INFN). It was distributed with additional software tools by the High-Energy Astrophysics Science Archive Research

Center (HEASARC) at NASA Goddard Space Flight Center (GSFC). M.M. acknowledges support from the research program Athena with project number 184.034.002, which is (partly) financed by the Dutch Research Council (NWO). M.M. has benefited from discussions during Team Meetings of the International Space Science Institute (Bern), whose support he acknowledges.

Appendix
Tables and Figures

In this appendix, we provide the results of the spectro-polarization analysis obtained using the PCUBE and XSPEC method for each segment of all Epochs in Table A1. We also show the evolution of time-averaged PA and PD with energy for all epochs in Figure A1.

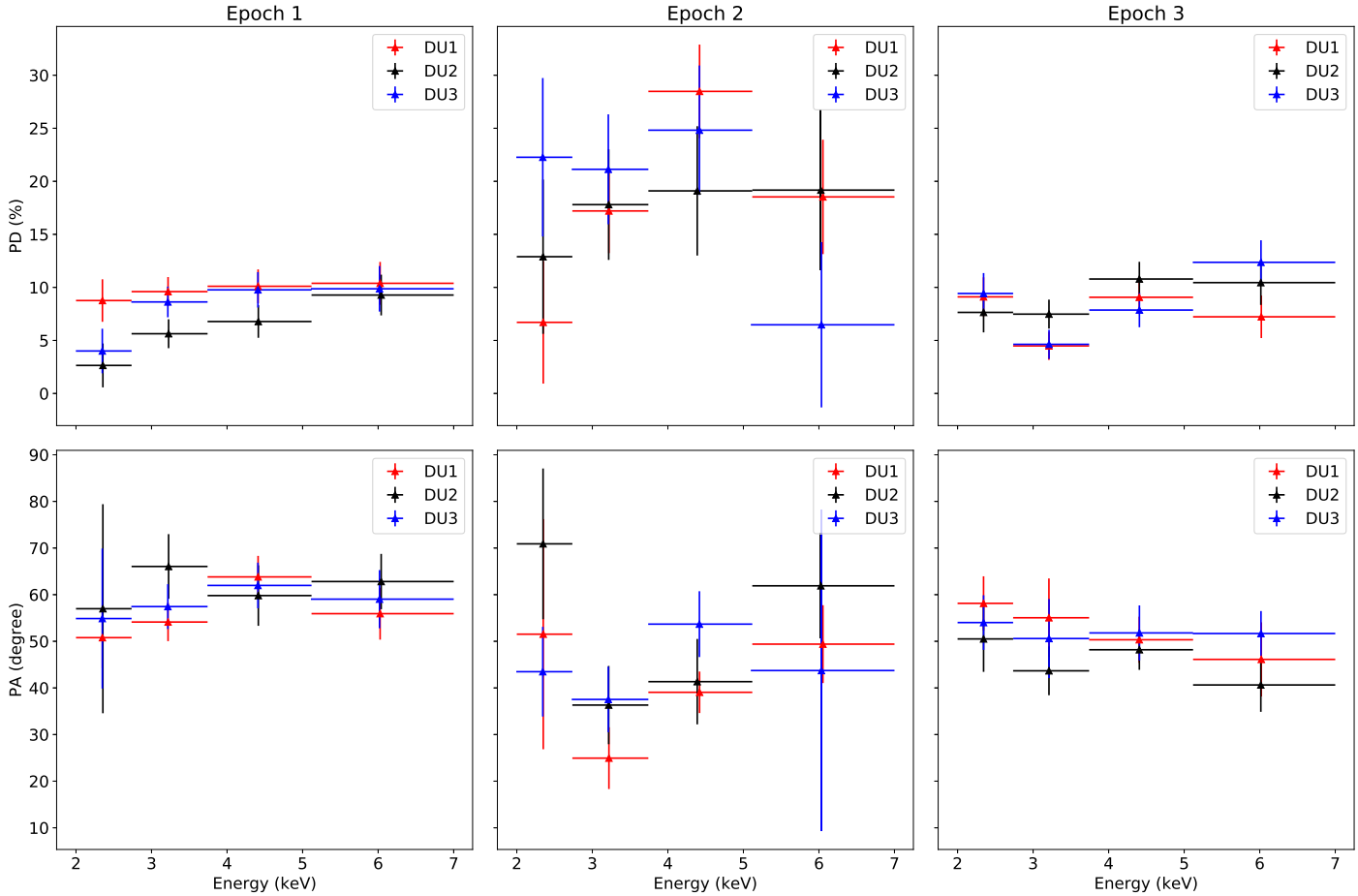

Figure A1. The PD and PA of Her X-1 as a function of energy for the three epochs.

Table A1

Epoch, Observation ID, Start and End Time of Observations with PA and PD Using Both PCUBE and XSPEC Model CONSTANT*POLCONST*POWERLAW, Power-law Index (Γ), POWERLAW Norm, and Goodness of the Fit for Her X-1

Epoch	Obs ID	Tstart (MJD)	Tstop (MJD)	PCUBE		XSPEC				
				PD (%)	PA (deg)	PD (%)	PA (deg)	Γ	Norm	χ^2 (dof)
1	01001899	59,628.55	59,628.82	14.1 ± 2.6	66.8 ± 5.3	14.9 ± 2.3	66.6 ± 4.4	0.42 ± 0.02	1.5 ± 0.0	594.5 (552)
		59,629.08	59,629.38	12.6 ± 2.0	65.4 ± 4.6	12.4 ± 1.8	66.8 ± 4.2	0.87 ± 0.01	4.5 ± 0.1	541.3 (552)
		59,629.88	59,630.31	6.4 ± 1.5	58.1 ± 6.8	5.9 ± 1.3	57.7 ± 6.6	0.94 ± 0.01	8.9 ± 0.1	587.5 (552)
		59,630.48	59,631.05	6.9 ± 1.2	67.0 ± 4.9	7.0 ± 1.0	60.6 ± 4.3	0.95 ± 0.01	14.9 ± 0.1	627.4 (552)
		59,631.49	59,631.65	7.1 ± 2.2	49.2 ± 8.8	7.8 ± 2.0	55.6 ± 7.2	0.96 ± 0.01	4.3 ± 0.1	570.4 (552)
		59,633.19	59,633.73	8.6 ± 1.3	56.5 ± 4.4	8.6 ± 1.2	58.5 ± 3.9	1.09 ± 0.01	13.7 ± 0.1	633.8 (552)
		59,633.77	59,634.26	8.9 ± 1.3	53.5 ± 4.2	9.3 ± 1.2	57.2 ± 3.6	1.08 ± 0.01	13.7 ± 0.1	596.4 (552)
		59,634.39	59,634.65	10.8 ± 3.0	41.5 ± 7.9	12.1 ± 2.7	42.3 ± 6.4	0.71 ± 0.02	1.6 ± 0.0	585.3 (552)
2	02003801	59,963.21	59,963.68	19.3 ± 2.8	43.1 ± 4.2	21.1 ± 2.5	39.8 ± 3.4	0.96 ± 0.02	4.5 ± 0.1	427.9(363)
		59,963.99	59,964.06	28.7 ± 8.0	60.0 ± 8.0	24.1 ± 7.2	42.7 ± 6.5	0.77 ± 0.06	0.4 ± 0.0	383.3 (363)
		59,964.88	59,965.30	13.5 ± 3.2	51.7 ± 6.8	16.1 ± 2.8	50.6 ± 5.1	0.74 ± 0.02	2.6 ± 0.1	325.8 (363)
3	02004001	59,978.83	59,979.12	9.0 ± 1.5	58.0 ± 4.7	8.2 ± 1.3	59.7 ± 4.5	0.99 ± 0.01	10.4 ± 0.1	575.8 (552)
		59,979.12	59,979.39	8.6 ± 1.7	56.8 ± 5.8	9.1 ± 1.5	64.5 ± 4.8	0.99 ± 0.01	7.3 ± 0.1	525.1 (552)
		59,980.04	59,980.51	8.8 ± 1.3	45.1 ± 4.4	6.6 ± 1.2	57.8 ± 5.1	0.98 ± 0.01	12.3 ± 0.1	637.9 (552)
		59,980.51	59,981.14	7.6 ± 1.2	47.0 ± 4.5	7.0 ± 1.0	49.6 ± 4.3	0.99 ± 0.01	15.5 ± 0.1	650.9 (552)
		59,981.77	59,982.27	9.5 ± 1.4	50.0 ± 4.2	7.4 ± 1.2	51.6 ± 4.7	1.01 ± 0.01	12.1 ± 0.1	466.9 (552)
		59,982.27	59,982.79	7.3 ± 1.7	46.5 ± 6.7	8.3 ± 1.5	37.0 ± 5.1	0.98 ± 0.01	7.6 ± 0.1	518.6 (552)
		59,983.44	59,983.92	14.2 ± 2.2	30.4 ± 4.4	17.1 ± 1.9	39.8 ± 3.2	0.93 ± 0.01	4.4 ± 0.1	588.4 (552)

ORCID iDs

Akash Garg https://orcid.org/0000-0002-7567-3475
Divya Rawat https://orcid.org/0000-0002-9280-2785
Yash Bhargava https://orcid.org/0000-0002-5967-8399
Mariano Méndez https://orcid.org/0000-0003-2187-2708
Sudip Bhattacharyya https://orcid.org/0000-0002-6351-5808

References

Abdallah, M. H., & Leahy, D. A. 2015, MNRAS, 453, 4222
Arnaud, K. A. 1996, in ASP Conf. Ser. 101, Astronomical Data Analysis Software and Systems V, ed. G. H. Jacoby & J. Barnes (San Francisco, CA: ASP), 17
Bala, S., Bhattacharya, D., Staubert, R., & Maitra, C. 2020, MNRAS, 497, 1029
Baldini, L., Barbanera, M., Bellazzini, R., et al. 2021, APh, 133, 102628
Baldini, L., Bucciantini, N., Lalla, N. D., et al. 2022, SoftX, 19, 101194
Becker, P. A., & Wolff, M. T. 2005, ApJL, 621, L45
Becker, P. A., & Wolff, M. T. 2007, ApJ, 654, 435
Caiazzo, I., & Heyl, J. 2021, MNRAS, 501, 129
dal Fiume, D., Orlandini, M., Cusumano, G., et al. 1998, A&A, 329, L41
Deeter, J. E., Boynton, P. E., & Pravdo, S. H. 1981, ApJ, 247, 1003
Di Marco, A., Fabiani, S., La Monaca, F., et al. 2022, AJ, 164, 103
Doroshenko, V., Poutanen, J., Tsygankov, S. S., et al. 2022, NatAs, 6, 1433
Fürst, F., Grefenstette, B. W., Staubert, R., et al. 2013, ApJ, 779, 69
Giacconi, R., Gursky, H., Kellogg, E., et al. 1973, ApJ, 184, 227
Gruber, D. E., Heindl, W. A., Rothschild, R. E., et al. 2001, ApJ, 562, 499
Igna, C. D., & Leahy, D. A. 2012, MNRAS, 425, 8
Ji, L., Staubert, R., Ducci, L., et al. 2019, MNRAS, 484, 3797
Kislat, F., Clark, B., Beilicke, M., & Krawczynski, H. 2015, APh, 68, 45
Kosec, P., Kara, E., Fabian, A. C., et al. 2022, ApJ, 936, 185
Leahy, D., & Wang, Y. 2020, ApJ, 902, 146
Leahy, D. A. 2002, MNRAS, 334, 847
Leahy, D. A. 2004, ApJ, 613, 517
Leahy, D. A., & Abdallah, M. H. 2014, ApJ, 793, 79
Muleri, F. 2022, in Handbook of X-ray and Gamma-ray Astrophysics, ed. C. Bambi & A. Santangelo (New York: Springer), 6
Petterson, J. A., Rothschild, R. E., & Gruber, D. E. 1991, ApJ, 378, 696
Rawat, D., Garg, A., & Méndez, M. 2023, arXiv:2303.02745
Scott, D. M., Leahy, D. A., & Wilson, R. B. 2000, ApJ, 539, 392
Shklovskij, I. S., & Efremov, Y. N. 1972, ATsir, 708, 1
Staubert, R., Klochkov, D., Vasco, D., et al. 2013, A&A, 550, A110
Tananbaum, H., Gursky, H., Kellogg, E. M., et al. 1972, ApJL, 174, L143
Weisskopf, M. C., Soffitta, P., Baldini, L., et al. 2022, JATIS, 8, 026002